

Investigation of Radiation Shielding Parameters of Certain Glass Materials Using Different Methods

ŞAHMARAN, Turan ¹, YAVUZKANAT, Nuray ²

¹ Kirikhan Vocational School, Hatay Mustafa Kemal University, Hatay, Turkey.

² Physics Department, Faculty of Art and Sciences, Bitlis Eren University, Bitlis, Turkey.

Correspondence:

Turan Şahmaran Kirikhan Vocational School, Hatay Mustafa Kemal University, Hatay, Turkey.
tsahmaran@gmail.com

Received: 19 February 2026

Revised: 21 March 2026

Accepted: 16 April 2026

ABSTRACT

Objective: In medical and industrial applications involving ionizing radiation, transparent shielding materials are essential for ensuring both safety and visual monitoring. This study comparatively evaluates the radiation shielding performance of three distinct glass matrices: Lead Glass (G-Pb), Plate Glass (G-Plate), and Pyrex Glass (G-Pyrex).

Methods and Materials: Shielding parameters, including Mass Attenuation Coefficient (MAC), Half-Value Layer (HVL), Mean Free Path (MFP), and Effective Atomic Number (Z_{eff}), were determined using Phy-X/PSD and MATHXCOM software across various energy levels. Additionally, the Effective Removal Cross-section was calculated to assess neutron shielding capabilities.

Findings: The results demonstrated that G-Pb exhibits significantly superior photon attenuation performance, particularly at low energies, attributed to its high lead content and effective atomic number. For instance, G-Pb showed much lower HVL and MFP values compared to the silicate-based G-Plate and G-Pyrex. Furthermore, G-Pb displayed remarkable neutron shielding efficiency, comparable to water, due to its high density (6.22 g/cm³).

Conclusion: The study concludes that while G-Plate and G-Pyrex are suitable for secondary barriers, G-Pb remains the primary choice for high-performance transparent shielding, such as diagnostic X-ray windows.

Keywords: Glass materials, effective atomic number, neutron protection, ionizing radiation

INTRODUCTION

Shielding is of paramount importance for occupational and environmental safety in medical imaging facilities, industrial radiography systems, and research laboratories where ionizing radiation is utilized (1-4). Shielding effectiveness varies depending on the type and energy of the radiation, the density and effective atomic number (Z_{eff}) of the material, as well as geometric conditions and thickness. In conventional shielding applications, lead (Pb) blocks and concrete structures are widely used due to their high densities and atomic numbers. However, the opaque nature of these materials poses a significant limitation in situations requiring visual monitoring of the radiation source or the patient by the staff (5,6). To overcome this limitation, there has been increasing interest in transparent shielding materials, particularly glass systems, which possess both optical transparency and high photon attenuation coefficients (7,8). Glass is generally a

silicate-based material with an amorphous structure, a characteristic that expands its range of applications. Various techniques and laminated structures have been employed to enhance the durability and impact resistance of glass (9-13). Glass materials can be optimized for shielding performance due to the modifiability of their chemical compositions and the ability to incorporate heavy metal oxides (HMO) (14-16). Accordingly, glass types such as borate, germinate, phosphate, silicate, and tellurite are widely used (16-18).

In this study, three fundamental glass types are prominent in industrial and medical applications due to their distinct properties-Plate Glass (standard plate/soda-lime glass), Pyrex Glass (borosilicate glass), and Lead Glass (Pb glass) are comparatively evaluated in terms of their radiation shielding performances. These three classes of glass stand out in practice when there is a need for transparent barriers (e.g., operator field of view, process monitoring, cabin windows). Plate Glass is

widespread and economical in architecture and industry, being primarily SiO₂–Na₂O–CaO based, whereas Pyrex Glass is known for properties such as chemical resistance and low thermal expansion (19,20).

While recent literature predominantly focuses on the synthesis and characterization of novel, complex heavy-metal oxide glass matrices, comprehensive comparative studies evaluating the shielding efficacy of widely accessible, standard commercial glasses using multiple modern computational methods remain limited. Therefore, differing from studies oriented towards new material synthesis, the main objective of this study is to provide a direct, dual-platform (Phy-X/PSD and MATXCOM) comparative evaluation of the broad-spectrum photon and fast-neutron shielding parameters of conventional Lead (G-Pb), Plate (G-Plate), and Pyrex (G-Pyrex) glasses. By doing so, this research aims to establish highly accurate, standardized reference data for these practical materials, facilitating their reliable selection and application in mixed-radiation environments.

The aim of this study is to comparatively investigate the attenuation performance of Lead Glass (G-Pb), Plate Glass (G-Plate), and Pyrex Glass (G-Pyrex) materials against X/gamma photons in environments requiring transparent shielding. In the evaluation, mass attenuation coefficient (μ/ρ), half-value layer (HVL), and tenth-value layer (TVL) and effective atomic number (Z_{eff}) values were determined using Phy-X/PSD and MATHXCOM software. In addition to these calculations, the effective removal cross-sections (Σ_R) of these materials were determined via MRCsC, Phy-X/PSD, and empirical methods.

MATERIAL AND METHODS

Linear Attenuation Coefficient (μ)

The linear attenuation coefficient expresses the probability of incoming photons interacting per unit path length within a material. It depends on the energy of the incoming radiation and the atomic number and density of the shielding material. It is calculated experimentally or theoretically using Beer-Lambert's law as follows:

$$I = I_0 e^{-\mu x} \quad (1)$$

$$\mu = \frac{1}{x} \ln \left(\frac{I_0}{I} \right) \quad (2)$$

where, I_0 is the incident radiation intensity; I is the radiation intensity passing through the material; and x (cm) is the sample thickness (Figure 1).

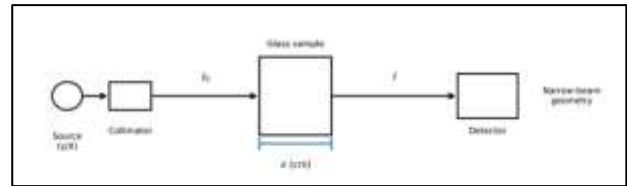


Figure 1: Schematic illustration of the narrow-beam attenuation geometry used in the photon shielding calculations based on Beer–Lambert law.

Mass Attenuation Coefficient (μ/ρ)

The mass attenuation coefficient is a fundamental parameter that indicates the ability of a material to absorb radiation, independent of its density. It is obtained by dividing the linear attenuation coefficient by the material density and is usually calculated using weight fractions for mixtures or compounds.

$$\mu_m = \frac{\mu}{\rho} = \sum w_i \left(\frac{\mu_i}{\rho_i} \right) \quad (3)$$

where, ρ is the density of the material (g/cm^3); w_i is the weight fraction of the i th element in the mixture, (μ_i/ρ_i) (cm^2/g) is the mass attenuation coefficient of the i th element.

Half-value and one-tenth value thickness (HVL/TVL)

The half-value thickness is the material thickness required to reduce the incoming radiation intensity to half (50%) of its initial value. It is a practical indicator of the shielding effectiveness of the material and is determined using the linear attenuation coefficient. The one-tenth value thickness indicates the shield thickness required to reduce the radiation intensity to one-tenth (10%) of the initial level.

$$HVL = \frac{\ln 2}{\mu} \quad (4)$$

$$TVL = \frac{\ln(10)}{\mu} = \frac{2.303}{\mu} \quad (5)$$

Mean free path (MFP)

The mean free path refers to the average distance a photon travels between two successive interactions within an absorbing material. This parameter indicates the penetration depth of radiation within the material and is calculated as the inverse of the linear attenuation coefficient.

$$MFP = \frac{1}{\mu} \quad (6)$$

Effective atomic number (Z_{eff})

The effective atomic number (Z_{eff}) is a quantity used to represent the interaction of multi-element compounds/composite materials with photons using a single equivalent atomic number, and it facilitates the comparison of shielding behavior, particularly in energy regions where the photoelectric effect is dominant.

$$Direct_{Z_{eff}} = \frac{\sum_i f_i A_i (\mu/\rho)_i}{\sum_j f_j \left(\frac{A_j}{Z_j} \right) (\mu/\rho)_j} \quad (7)$$

$$\sigma_a = \frac{(\mu/\rho)_m}{N \sum_i (W_i/A_i)} \quad (8)$$

$$Interpolation_{Z_{eff}} = \frac{Z_1(\log \sigma_2 - \log \sigma_a) + Z_2(\log \sigma_a - \log \sigma_1)}{\log \sigma_2 - \log \sigma_1} \quad (9)$$

where, f_i, molar fraction of element i in the material; A_i, atomic weight of element i; N, Avogadro's number; σ_a atomic cross section.

Effective Removal Cross-section (Σ_R)

This parameter defines the probability of the material attenuating fast neutrons (via elastic or inelastic scattering).

$$\Sigma_{R/\rho} = 0.190 Z^{-0.743} \quad Z \leq 8 \text{ and } \Sigma_{R/\rho} = 0.125 Z^{-0.565} \quad Z > 8 \quad (10)$$

$$\Sigma_R = \sum_i \rho_i (\Sigma_{R/\rho})_i \quad (11)$$

$$\rho_i = w_i \rho_m \quad (12)$$

where (Σ_R/ρ)_i is the mass removal cross section of the ith component, ρ_m is the material density, ρ_i is partial density. w_i is the weight ratio of the compound or element.

Computing programs

In this study, two independent computational methods, Phy-X/PSD and MATXCOM, were utilized to evaluate the radiation shielding parameters. Phy-X/PSD (21) is a comprehensive, web-based software widely recognized for rapidly calculating various shielding parameters over a broad continuous energy range, including the effective removal cross-section (Σ_R) for fast neutrons. On the other hand, MATXCOM (22) is a recently developed analytical tool that relies on the updated EPICS2023 evaluated photon data library to determine accurate X-ray and gamma-ray attenuation parameters. The primary rationale for employing both software programs together is to conduct a rigorous cross-verification of the results obtained. By comparing the theoretical outputs from these two distinct computational approaches and fundamental data libraries, the study ensures enhanced accuracy, eliminates potential software-based calculation anomalies, and provides highly reliable data regarding the shielding capacities of the investigated glass materials.

Table 1. Elemental fractions of the materials.

Materials	G-Pb	G-Pyrex	G-Plate
B	-	0.0401	0.4598
O	0.1565	0.5396	-
Na	-	0.0282	0.0964
Al	-	0.0116	-
Si	0.0809	0.3772	0.3366
K	-	0.0033	-
Ti	0.0081	-	-
As	0.0027	-	-
Pb	0.7519	-	-
Ca	-	-	0.1072
Density (g/cm ³)	6.22	2.23	2.40

Table 2. Variation of MAC with MATHXCOM and Phy-X/PSD at different energies.

Sources	Energy (keV)	G-Pb		G-Pyrex		G-Plate	
		Phy-X/PSD	MATHXCOM	Phy-X/PSD	MATHXCOM	Phy-X/PSD	MATHXCOM
Am-241	59.54	3.918	3.920	0.244	0.242	0.294	0.292
-	80	1.870	1.821	0.189	0.190	0.209	0.208
-	100	4.215	4.216	0.166	0.165	0.176	0.175
Eu-152	121.78	2.580	2.582	0.151	0.150	0.157	0.156
-	200	0.782	0.783	0.125	0.124	0.126	0.125
-	300	0.330	0.329	0.107	0.106	0.107	0.106
I-131	364	0.231	0.229	0.099	0.098	0.099	0.101
-	400	0.198	0.198	0.095	0.095	0.096	0.097
-	500	0.143	0.142	0.087	0.086	0.087	0.088
Cs-137	662	0.102	0.100	0.077	0.076	0.077	0.078
Co-60	1175	0.061	0.060	0.058	0.057	0.059	0.060
Co-60	1333	0.056	0.058	0.054	0.053	0.055	0.056
Eu-152	1408.01	0.054	0.052	0.051	0.050	0.053	0.054

Table 3. Variation of HVL/TVL with Phy-X/PSD and MATHXCOM at different energies.

Sources	Energy (keV)	G-Pb		G-Pyrex		G-Plate	
		Phy-X/PSD	MATHXCOM	Phy-X/PSD	MATHXCOM	Phy-X/PSD	MATHXCOM
Am-241	59.54	0.028/0.094	0.027/0.095	1.275/4.237	1.274/4.236	0.992/3.296	0.991/3.295
-	80	0.060/0.198	0.059/0.197	1.645/5.463	1.644/5.462	1.384/4.598	1.383/4.597
-	100	0.026/0.088	0.027/0.199	1.875/6.230	1.876/6.231	1.641/5.453	1.640/5.451
Eu-152	121.78	0.043/0.143	0.042/0.144	2.056/6.830	2.055/6.828	1.840/6.113	1.841/6.114

-	200	0.142/0.473	0.141/0.474	2.494/8.284	2.492/8.281	2.290/7.608	2.890/7.606
-	300	0.338/1.122	0.339/1.124	2.906/9.655	2.905/9.654	2.687/8.926	2.686/8.925
I-131	364	0.482/1.600	0.483/1.598	3.138/10.425	3.139/10.426	2.906/9.653	2.905/9.652
-	400	0.562/1.866	0.560/1.864	3.258/10.823	3.259/10.825	3.018/10.027	3.017/10.025
-	500	0.780/2.590	0.790/2.591	3.574/11.874	3.572/11.872	3.314/11.010	3.315/11.011
Cs-137	662	1.093/3.630	1.094/3.640	4.041/13.423	4.040/13.422	3.749/12.454	3.748/12.452
Co-60	1175	1.828/6.071	1.827/6.070	5.311/17.641	5.310/17.640	4.930/16.378	4.931/16.379
Co-60	1333	1.996/6.631	1.995/6.630	5.669/18.831	5.671/18.833	5.262/17.480	5.260/17.478
Eu-152	1408.01	2.064/6.857	2.063/6.855	5.831/19.369	5.830/19.368	5.510/18.303	5.511/18.304

Table 4. Variation of MFP with Phy-X/PSD and MATHXCOM at different energies.

Sources	Energy (keV)	G-Pb		G-Pyrex		G-Plate	
		Phy-X/PSD	MATHXCOM	Phy-X/PSD	MATHXCOM	Phy-X/PSD	MATHXCOM
Am-241	59.54	0.041	0.040	1.840	1.841	1.431	1.430
-	80	0.086	0.085	2.373	2.374	1.997	1.996
-	100	0.038	0.037	2.705	2.706	2.368	2.366
Eu-152	121.78	0.062	0.061	2.966	2.965	2.655	2.654
-	200	0.206	0.205	3.598	3.599	3.304	3.305
-	300	0.407	0.406	4.193	4.192	3.877	3.878
I-131	364	0.695	0.693	4.527	4.526	4.192	4.193
-	400	0.810	0.811	4.700	4.701	4.355	4.356
-	500	1.125	1.124	5.157	5.155	4.781	4.780
Cs-137	662	1.577	1.575	5.829	5.830	5.409	5.408
Co-60	1175	2.637	2.635	7.662	7.661	7.113	7.111
Co-60	1333	2.880	2.881	8.178	8.177	7.592	7.590
Eu-152	1408.01	2.978	2.976	8.564	8.562	7.808	7.809

Table 5. Variation of Zeff with Phy-X/PSD and MATHXCOM at different energies.

Sources	Energy (keV)	G-Pb		G-Pyrex		G-Plate	
		Phy-X/PSD	MATHXCOM	Phy-X/PSD	MATHXCOM	Phy-X/PSD	MATHXCOM
Am-241	59.54	73.88	73.87	10.21	10.20	11.93	11.92
-	80	69.28	69.29	9.84	9.83	11.26	11.26
-	100	76.47	76.46	9.68	9.67	10.93	10.93
Eu-152	121.78	73.97	73.98	9.59	9.60	10.75	10.74
-	200	63.20	63.21	9.49	9.50	10.54	10.54
-	300	51.04	51.03	9.47	9.48	10.49	10.48
I-131	364	45.52	45.52	9.46	9.47	10.47	10.46
-	400	43.15	43.14	9.45	9.44	10.47	10.46
-	500	38.33	38.33	9.45	9.44	10.46	10.46

Cs-137	662	33.69	33.68	9.44	9.44	10.46	10.46
Co-60	1175	29.30	29.30	9.44	9.43	10.45	10.45
Co-60	1333	28.33	28.33	9.44	9.43	10.45	10.45
Eu-152	1408.01	28.78	28.78	9.44	9.43	10.45	10.45

RESULTS and DISCUSSION

Elemental fractions and density of the materials are detailed in Table 1. The shielding parameters of the materials were examined using the MATHXCOM and Phy-X/PSD programs.

A higher MAC indicates a superior ability of the material to shield against or stop radiation (Table 2). The MAC values of the G-Pb material are significantly higher compared to the other two samples. This difference becomes particularly pronounced at low energies. For instance, at 59.54 keV, the value for G-Pb is 3.918, whereas the others range between approximately 0.24 and 0.29. G-Pb contains a high concentration of the element Lead (Pb). Due to the high atomic number (Z) of heavy elements, they stop radiation much more effectively at low energies through the photoelectric effect. G-Plate provides slightly better shielding than G-Pyrex at low energy levels (e.g., between 59.54 - 100 keV) (0.294 vs. 0.244). However, as energy increases (e.g., 662 keV and above), this difference diminishes, and the values converge (both are ~ 0.077 for the Cs-137 source). At high energies, shielding capability becomes more dependent on density rather than atomic number, leading to a narrowing of the difference between the materials. When comparing the Phy-X/PSD and MATHXCOM results for each row and column in Table 2, it is observed that the values are almost identical; the difference between the results is less than 1%. The K-shell absorption edge of the Pb element within the G-Pb sample is approximately 88 keV. The energy of the incident photon (80 keV) is insufficient to eject electrons from the innermost shell (K-shell) of the lead atom (since $80 < 88$ keV). Consequently, the probability of interaction decreases, and the MAC value follows the normal declining trend, dropping to 1.87. Once the photon energy surpasses the 88 keV threshold (e.g., at 100 keV), it becomes capable of ejecting electrons from the K-shell. When this new interaction channel opens, the absorption probability (cross-section) exhibits a sudden jump, and the value increases from 1.87 to 4.21. The reason for the lower value observed at 80 keV is that it falls just below the K-absorption edge limit (88 keV) of the Pb element present in the material.

The values presented in Table 3 indicate the material thickness required to reduce the radiation intensity to half and one-tenth of its initial value. G-Pb demonstrates significantly superior shielding performance compared to the other two materials. This is because lower HVL and TVL values correspond to a greater capability of the material to stop radiation. For instance, for the Cs-137 (662 keV) source, the HVL value of G-Pb is approximately 1.093 cm, whereas it is 4.041 cm for G-Pyrex and 3.749 cm for G-Plate. This implies that to achieve the same level of protection using G-Pyrex, a glass thickness nearly four times that of G-Pb is required. The HVL and TVL values for all materials increase as the energy increases. This is an expected physical phenomenon, as high-energy photons penetrate matter more easily. However, even at high energies (e.g., Co-60, 1333 keV), G-Pb provides protection at significantly lower thicknesses compared to the others.

MFP represents the average distance a photon travels before interacting with matter. A lower MFP value indicates superior shielding capability. The data presented in Table 4 corroborate the findings in Table 3. G-Pb exhibits the lowest MFP values. At low energies, such as with Am-241 (59.54 keV), the MFP value for G-Pb is 0.041 cm, whereas it is 1.840 cm for G-Pyrex. This indicates that the probability of lead-doped glass (G-Pb) interacting with radiation at low energies is significantly higher than that of standard glasses. Although G-Plate demonstrates slightly better performance (lower MFP) compared to G-Pyrex, both exhibit weak performance when compared to G-Pb.

Z_{eff} is the calculated atomic number derived under the assumption that a material behaves as a single element during its interaction with radiation (Table 5). A high Z_{eff} implies a superior radiation absorption capacity. G-Pb exhibits a remarkably high Z_{eff} value of approximately 73.88 at an energy of 59.54 keV. This serves as the strongest evidence of the high Pb content within the material. In contrast, the other materials (G-Pyrex and G-Plate) remain within the 9-12 range, displaying characteristics typical of silicate-based glasses. Although the Z_{eff} value of G-Pb decreases with increasing energy

(dropping from 73 to 28), it remains superior to the other two materials (approximately 9-10) even at its lowest level.

As observed in Table 6, Water and G-Pb exhibit the highest ΣR values among the materials. Water possesses the highest value of 0.1102 cm^{-1} according to the MRCsC method. Water serves as a standard reference material for neutron moderation due to its high hydrogen content, and as expected, it demonstrated superior performance. Remarkably, G-Pb, a glass type characterized by a very high density of 6.22 g/cm^3 exhibits a performance very close to that of water, with ΣR values ranging from 0.103 to 0.105 cm^{-1} . Generally, heavy elements are less effective in neutron shielding compared to hydrogenous materials. However, due to its high density, G-Pb possesses a higher ΣR value resulting from an increased probability of interaction per unit volume. This indicates that G-Pb could be a viable candidate for transparent neutron shielding in space-constrained environments (situations requiring thin shielding). Although the densities of G-Pyrex and G-Plate are comparable to concrete ($2.23 - 2.40 \text{ g/cm}^3$), their neutron shielding capabilities are inferior. This suggests that the chemical compositions of these glasses are not optimized for neutron shielding purposes.

The MAC values of G-Pb are in agreement with previously reported high-density heavy metal oxide glasses. At 662 keV, G-Pb exhibits a MAC of $0.102 \text{ cm}^2/\text{g}$, which aligns with the MAC value of $0.100 \text{ cm}^2/\text{g}$ reported by Kurudirek (2017) for lead-bismuth-borate glasses (11). The Zeff trend of G-Pb also mirrors typical heavy metal-doped glasses, characterized by a sharp decline in the intermediate energy regions where Compton scattering takes precedence over the photoelectric effect. Furthermore, the results obtained for the silicate-based G-Plate and G-Pyrex glasses follow the attenuation trends reported for conventional soda-lime and borosilicate glasses. Kuluöztürk (2023) calculated the MAC of a standard soda-lime glass to be $\sim 0.0769 \text{ cm}^2/\text{g}$ at 662 keV, which correlates with our finding of $0.077 \text{ cm}^2/\text{g}$ for G-Plate at the same energy level (20). Similar photon energy-dependent behaviors were also validated by Kurtuluş et al. (2020) for waste soda-lime-silica glasses, confirming that structural densities dictate high-energy attenuation capacities (13). Lastly, the effective removal cross-section of G-Pb demonstrates a fast-neutron shielding performance consistent with established heavy metal-containing glasses. While typical heavy metal oxide systems, such as the BaO/SrO-Bi₂O₃-B₂O₃ glasses investigated by Sayyed

et al. (2018), exhibit ΣR values in the range of 0.092 to 0.106 cm^{-1} , the density of G-Pb (6.22 g/cm^3) ensures a comparable macroscopic cross-section (14). This quantitative alignment with the literature affirms that G-Pb is not only an effective barrier for diagnostic X-rays but also a comprehensive protective transparent medium against mixed radiation fields.

CONCLUSION

In this study, G-Pb, G-Pyrex, and G-Plate materials were compared from the perspective of transparent shielding. G-Pb materials, defined by lead equivalence, should be the primary choice for diagnostic X-ray windows requiring high shielding levels. G-Pyrex may offer advantages in environments where thermal shock or chemical resistance is critical, but where shielding requirements are lower or of secondary importance. As an economical and widespread solution, G-Plate can be considered for secondary barriers or applications with low shielding requirements; however, since thickness requirements may increase with rising energy, the design must be verified based on HVL/TVL parameters. Decisions in transparent shielding design should not rely solely on attenuation parameters but must be based on a comprehensive evaluation of criteria such as thickness, weight, mechanical load-bearing capacity, and compliance with standards.

Conflict of Interest

There are no conflicts of interest and no acknowledgements.

References

1. Kurudirek M, Chutithanapanon N, Laopaiboon R, Yenchai C, Bootjomchai C, Effect of Bi₂O₃ on Gamma ray Shielding and Structural Properties of Borosilicate Glasses Recycled from High Pressure Sodium Lamp Glass. *J. Alloys Compd.* 2018, 745, 355–64. <https://doi.org/10.1016/j.jallcom.2018.02.158>.
2. Tekin HO, Sayyed MI, Issa SA. Gamma radiation shielding properties of the hematite-serpentine concrete blended with WO₃ and Bi₂O₃ micro and nano particles using MCNPX code. *Radiation Physics and Chemistry.* 2018;1(150):95-100. <https://doi.org/10.1016/j.radphyschem.2016.09.019>.
3. Yavuzkanat N, Şahmaran T. Analyzing neutron and gamma ray shielding properties in varied W-B₂O₃ ratios: methodological comparisons and

Monte Carlo simulation. *Radiation Effects and Defects in Solids*. 2024; 1(179):1697-710.

4. Kaşkaş A, Şahmaran T. Determination of the radiological properties of materials: A new approximation method for calculation of the mass attenuation coefficients. *Applied Radiation and Isotopes*. 2022; 1(187):110340. <https://doi.org/10.1016/j.apradiso.2022.110340>.

5. Sayyed MI, Rammah YS, Abouhaswa AS, Tekin HO, Elbashir BO. ZnO-B₂O₃-PbO glasses: synthesis and radiation shielding characterization. *Physica B: Condensed Matter*. 2018; 1(548):20-6. <https://doi.org/10.1016/j.physb.2018.08.024>.

6. Es-soufi, H., Ouachouo, L., Sayyed, M.I., Hashim, S., Bih, H., Bih, L., 2023. Synthesis and investigation of the physical, structural, and radiation shielding properties of the titano-bismuth phosphate glasses. *J. Mater. Sci. Mater. Electron*. 2023; 34(12):10479-7. <https://doi.org/10.1007/S10854-023>.

7. McCaffrey JP, Tessier F, Shen H. Radiation shielding materials and radiation scatter effects for interventional radiology (IR) physicians. *Medical physics*. 2012; 7(39):4537-46.

8. AbuAlRoos NJ, Amin NA, Zainon R. Conventional and new lead-free radiation shielding materials for radiation protection in nuclear medicine: A review. *Radiation Physics and Chemistry*. 2019; 1;165:108439. <https://doi.org/10.1016/j.radphyschem.2019.108439>

9. Kara Ü, Şahmaran T, Yavuzkanat N. Comprehensive Study on Gamma-Ray, Neutron, and Charged Particle Shielding Properties of Glass Materials Using Analytical Methods and Monte Carlo Simulations. *Nuclear Technology*. 2025; 5(18):1-20. <https://doi.org/10.1080/00295450.2025.2476342>.

10. Sayyed MI, Elhouichet H. Variation of energy absorption and exposure buildup factors with incident photon energy and penetration depth for boro-tellurite (B₂O₃-TeO₂) glasses. *Radiation physics and chemistry*. 2017; 1 (130):335-42. <https://doi.org/10.1016/j.radphyschem.2016.09.019>.

11. Kurudirek M. Heavy metal borate glasses: potential use for radiation shielding. *Journal of Alloys and Compounds*. 2017; 15(727):1227-36. <https://doi.org/10.1016/j.jallcom.2017.08.237>.

12. Yavuzkanat N. Exploring radiation shielding properties of lanthanide elements. *Bitlis Eren Üniversitesi Fen Bilimleri Dergisi*. 2024;13(4):1314-24. <https://doi.org/10.17798/bitlisfen.1558208>.

13. Kurtulus R, Kavas T, Akkurt I, Gunoglu K, 2020. An experimental study and WinXCom calculations on X-ray photon characteristics of Bi₂O₃- and Sb₂O₃-added waste soda-lime-silica glass. *Ceram. Int*. 2020;46 (13): 21120–21127. <https://doi.org/10.1016/j.ceramint.2020.05.188>.

14. Sayyed MI, Lakshminarayana G, Dong MG, Ersundu MÇ, Ersundu AE, Kityk IV. Investigation on gamma and neutron radiation shielding parameters for BaO/SrO–Bi₂O₃–B₂O₃ glasses. *Radiation Physics and Chemistry*. 2018; 1(145):26-33. <https://doi.org/10.1016/j.radphyschem.2017.12.010>.

15. Dong M, Xue X, Yang H, Liu D, Wang C, Li Z. A novel comprehensive utilization of vanadium slag: As gamma ray shielding material. *Journal of hazardous materials*. 2016; 15(318):751-7. <https://doi.org/10.1016/j.jhazmat.2016.06.012>.

16. Varshneya A.K, Mauro J.C. *Fundamentals of Inorganic Glass Making*. 2019. <https://doi.org/10.1016/b978-0-12-816225-5.00022-5>.

17. Karasu B, Bereket O, Biryani E, Sanoglu D. The latest developments in glass science and technology. *El-Cezeri Fen ve Mühendislik Derg*. 2017; 4(2): 209–233. <https://doi.org/10.31202/ecjse.318204>.

18. Kurtulus R. Recent developments in radiation shielding glass studies: a mini review on various glass types. *Radiation Physics and Chemistry*. 2024; 1(220):111701. <https://doi.org/10.1016/j.radphyschem.2024.111701>

19. Phillips JC, Kerner R. Structure and function of window glass and Pyrex. *The Journal of Chemical Physics*. 2008;128(17): 174506. <https://doi.org/10.1063/1.2805043>.

20. Kuluöztürk ZN. Gamma-ray shielding properties of soda-lime glass and glass ceramic: an experimental and Monte Carlo simulation study. *Radiation Physics and Chemistry*. 2023; 1(212):111172.

21. Şakar E, Özpolat ÖF, Alım B, Sayyed MI, Kurudirek M. Phy-X/PSD: development of a user friendly online software for calculation of parameters relevant to radiation shielding and dosimetry. *Radiation Physics and Chemistry*. 2020;(166): 108496. <https://doi.org/10.1016/j.radphyschem.2019.108496>

22. Islam, S. MATXCOM-an x-ray/gamma-ray attenuation calculator for arbitrary materials based on EPICS2023 evaluated photon data library. *Radiation Physics and Chemistry*, 2025; (229):

112433.

<https://doi.org/10.1016/j.radphyschem.2024.112433>

23. El-Samrah MG, El-Mohandes AM, El-Khayatt AM, Chidiac SE. MRCsC: A user-friendly software for predicting shielding effectiveness against fast neutrons. *Radiation Physics and Chemistry*. 2021(182): 109356.
<https://doi.org/10.1016/j.radphyschem.2021.109356>